Tunable plasmon-induced transparency effect based on self-asymmetric H-shaped resonators meta-atoms

2015 J. Opt. 17 035103

(http://iopscience.iop.org/2040-8986/17/3/035103)

IOP Publishing Journal of Optics
J. Opt. 17 (2015) 035103 (6pp) doi:10.1088/2040-8978/17/3/035103

Tunable plasmon-induced transparency effect based on self-asymmetric H-shaped resonators meta-atoms

Zhaoxiang Cheng, Lin Chen, Xiaofei Zang, Bin Cai, Yan Peng and Yiming Zhu

Shanghai Key Lab of Modern Optical System, Engineering Research Center of Optical Instrument and System, Ministry of Education, University of shanghai for Science and Technology, 516 Jungong Road, Shanghai 200093, People's Republic of China

E-mail: linchen@usst.edu.cn and ymzhu@usst.edu.cn

Received 27 October 2014, revised 25 December 2014
Accepted for publication 5 January 2015
Published 13 February 2015

Abstract

We have proposed and demonstrated a tunable plasmon-induced transparency (PIT) effect from two ways, based on self-asymmetric H-shaped resonators (AHR) meta-atoms. The tunable PIT effect is realized via varying polarization angles and coupling distances. First, by proper design, transition from PIT mode to dipole mode is theoretically and experimentally demonstrated by simply adjusting the polarization angle. Also, the manipulation of 'dark-mode' resonance intensity from strong to weak is achieved by varying coupling strength with different distances, which provided insight into the magnetic coupling hybridization mechanism. Prospectively, due to its special tunable characteristics, the AHR meta-atoms may be widely used in slow light, filters and switch devices.

Keywords: metamaterials, electromagnetic optics, polarization, resonance

(Some figures may appear in colour only in the online journal)

1. Introduction

Metamaterials have been an interest of researchers in recent years due to their fantastic characteristics and potential applications, such as use in negative refractive indices [1, 2], absorbers [3, 4], superlenses [5], filters [6, 7], and cloaking devices [8]. The electromagnetic behaviors of metamaterials can also be engineered to mimic the electromagnetically induced transparency (EIT) of atomic systems [9, 10]. EIT is a quantum effect that refers to the formation of a sharp transmission window, which is caused by the destructive interference between two different excitation routes of atomic states. In general, most EIT-like, also called plasmon-induced transparency (PIT) effects, realized in metamaterials (or meta-atoms) are based on two mechanisms: the bright-dark coupling and the trapped mode resonance (or sup-radiant and sub-radiant mode interference). The first one controls the coupling between a bright mode and a dark mode. The bright component can be directly excited by the incident electromagnetic field, while the dark one responds indirectly though the coupling with the bright one. The second approach is created by the symmetry breaking of the structure to activate a resonance with an anti-symmetric current configuration (or destructive interference between broad and narrow resonance spectra). The PIT behaviors achieved through these two approaches both result from destructive interference. Normally, researchers focus on the realization of some exotic characteristics based on PIT metamaterials [11–20], such as a broadband spectral range [11], polarization-independent transmission spectra [12, 13], multi-transparency peak [14], tunable transmission property [15, 16], and so on. The manipulation of the PIT effect is a key issue, which provides a broad application in terahertz (THz) and microwave region, such as tunable filters, sensors, and switch devices. Although the tunable PIT properties have already been achieved by special design of sample or doping light-activated (or electro-sensitive) materials [15, 16], a simple and practical way to realize tunable PIT effect is still desirable. In this paper, we

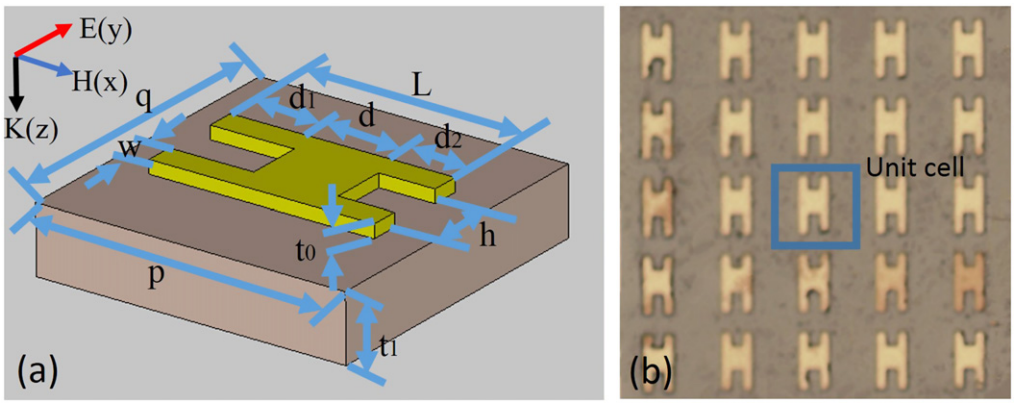

Figure 1. (a) The unit cell of structure, length L = 80 μm, central bar distance d = 30 μm, left depth d_1 = 30 μm, right depth d_2 = 20 μm, slot width h = 40 μm, line width w = 10 μm, the thickness of aluminum and substrate is t_0 = 0.2 μm, t_1 = 500 μm, respectively, and the period p = q = 110 μm. (b) Optical microscope images of the AHR sample.

study the tunable PIT effect based on self-asymmetric H-shaped resonator (AHR) meta-atoms structure, which can be widely used as a simple construction to achieve various applications [21–23]. Different from realizing a broadband transparency peak by fabricating different depths of the resonators [23], we prefer to emphasize the tunable PIT effect with different polarization angles and varied coupling distances. First, the PIT mode and dipole mode are observed to be excited by an incident plane wave with a 0° and 45° polarization angle, respectively. By proper design of the metamaterials structure, the transition from switch-on state (PIT mode) to switch-off state (dipole mode) can be achieved by simply adjusting the polarization angle. Also, the manipulation of dark-mode resonance intensity is achieved by controlling the coupling strength with varying distances, which provide insight into the magnetic coupling mechanism. Consequently, as it is simply a tunable transmission effect, the AHR meta-atoms' structures may have promising applications in filters, sensors, and slow light devices.

2. Sample design and fabrication

The designed PIT meta-atom structure is an AHR scheme, as shown in figure 1. The geometric parameters of the unit cell are depicted in figure 1(a), with length L = 80 μm, slot width h = 40 μm, line width w = 10 μm, and the period p = q = 110 μm. The left resonator has a depth d_1 = 30 μm and the right resonator has a depth d_2 = 20 μm; there is a central bar distance of d = 30 μm. The meta-atom structure was fabricated with 200 nm thick aluminum on a 500 μm thick n-type silicon substrate by conventional photolithography [24]. Figure 1(b) is the photograph of the experimental sample. The planar samples were measured by using fast and slow scan-based THz time domain spectroscopy (THz-TDS) [25–27]. The amplitude transmission spectra $|t(\omega)| = |E_S(\omega)/E_R(\omega)|$ were measured under normal incidence (k//z) with electric field E parallel to the *Y* axis(E//y, H//x), where $E_S(\omega)$ and $E_R(\omega)$ are Fourier transformed amplitudes of the THz pulse transmitted through the samples and reference (the blank silicon substrate), respectively. The measured data are supported by full-wave numerical simulation computer simulation technology (CST) Microwave Studio with Frequency Domain solver (FD) using unit cell boundaries in the x and y direction along with Floquet ports [28]. Specially, to remove the Fabry Pérot echo caused by the silicon substrate, we selected an 'open add space' boundary in the +z direction and an 'open' boundary in the −z direction. This means there is a half space in the z direction in our FD simulation: on top of the substrate, there is an AHR structure, followed by an open add space boundary; on the back of the sample, there is only the dielectric followed by an open boundary. In such an ideal interface, there will be no Fabry Pérot echo because there is only one face. The silicon substrate was modeled as a lossless dielectric $\varepsilon_{si} = 11.78$ since its loss is very low in the THz region, and Al was simulated with a default conductivity of $\sigma_{Al} = 3.56 \times 10^7$ S m^{-1}, which behaves almost like a perfect conductor, compared to the visible region [29].

3. Result and discussions

3.1. Transition between PIT mode and dipole mode by varying polarization angle

First, we investigate the transmission response of the AHR structure under the normal incident plane wave with various polarization angles $\theta = 0°$, 45°, and 90°. The experimental transmission spectra with different polarization angles are given in figure 2. The insert image in figure 2 is the schematic view of the varying polarization angle θ. As illustrated in figure 2, in the absence of rotating, i.e., $\theta = 0°$, a transparency peak located at 0.72 THz appears between two resonance dips at 0.65 THz and 0.79 THz (black curve). With the increase of polarization angle θ, the transmission peak intensity declines and the high-frequency resonance dip gradually disappears and eventually, when $\theta = 90°$, the spectrum degenerates to a transmission dip at 0.72 THz and the transparency peak disappears (green curve).

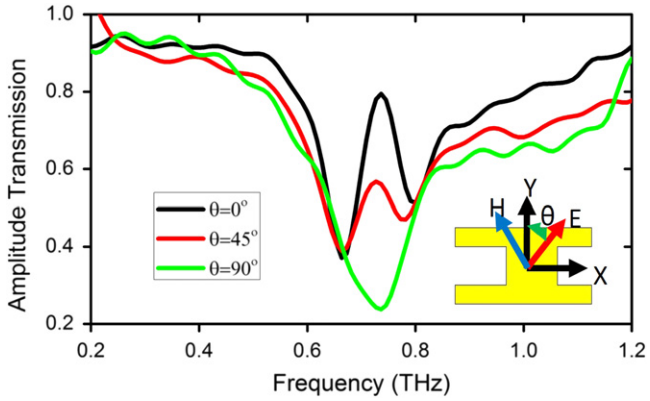

Figure 2. (a) Experimental transmission spectra of the AHR structure with various polarization angles $\theta = 0°$ (black curve), 45° (red curve), and 90° (green curve). The insert image is the scheme of varying polarization angle θ.

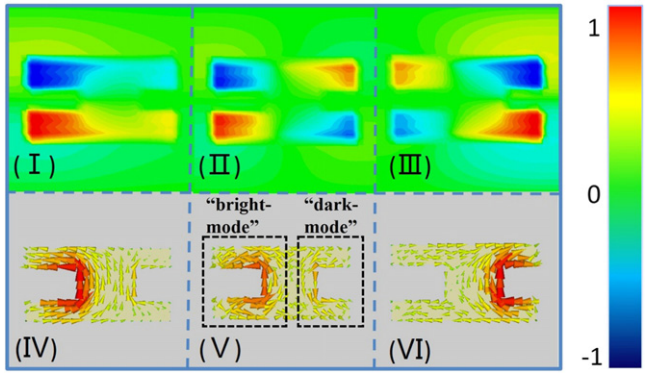

Figure 4. The electric field and surface current distributions with 0° polarization angle (I) and (IV) at the first resonance dip at 0.65 THz, (II) and (V) at the transparency peak 0.72 THz (III) and (VI) at the second resonance dip 0.79 THz.

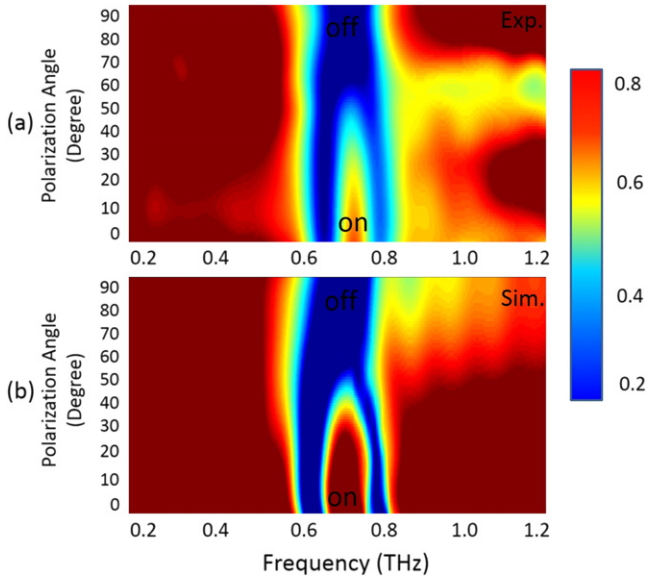

Figure 3. (a) The experimental and (b) simulated transmission spectra by varying polarization angle θ from 0° to 90°.

To gain overall insight of the polarization characteristics, the experimental and simulated transmission spectra under different polarization angle varying from 0° to 90° are exhibited in figure 3. A transition between the switch-on state and switch-off state can be observed clearly with different polarization angles. On the hand, the transparency window exists when polarization angle $\theta = 0°$, which can be regarded as the switch-on state. On the other hand, the transparency peak fades gradually with the increase of polarization angle θ. When θ is increased to 90°, only a resonance dip exists and the transparency peak disappears, which can be viewed as a switch-off state.

To research the underlying mechanism of the transmission response, the electric field and surface current distributions are given below. To start with, we try to study the origin of the transparency spectral characteristics with 0° polarization angle, as shown in figure 4. The electric field and surface current distributions are shown in figure 4. As explained by magnetic-dipole-induced transparency mechanism in [23], a PIT effect can be observed in figure 4. The low-frequency resonance dip dominantly arises from the induction-capacitance (LC) resonance of the deeper resonator (left side), and an counterclockwise surface current emerges at the left depth, which is in accordance with the excited electric field, as shown in figure 4 in (I) and (IV). The LC resonance on the shallower resonator (right side) evokes the high-frequency resonance dip with clockwise flowing surface currents around the right depth, as shown in figure 4 in (III) and (VI). At the transparency peak (see figures 4 (II) and (V)), the surface currents remain counterclockwise for the left depth, while the currents in the right depth change to be counterclockwise. Therefore, the left depth can be regarded as a 'bright mode' owing to in-phase currents with the excited electric field, while the right depth is a dark mode due to its anti-phase surface currents, as shown in figure 4(V). Consequently, a PIT transmission spectrum is observed as the energy excited in the bright mode transfers to the dark mode with low-energy dissipation. In addition, we marked the bright and dark mode clearly in figure 4.

Then, the electric field and surface current distributions at the resonance dip with 90° polarization angle are given in figure 5(a). It is a typical dipole mode at the resonance dip (0.72 THz) as a parallel electric field to the arms of an AHR structure. Next step, we focus on the coupling property with a 45° polarization angle, as shown in figure 5(b). The parallel electric field component (E//y) brings about the transparency peak at 0.72 THz, owing to PIT mode. Meanwhile, a resonance dip at the same frequency (0.72 THz) is evoked by the dipole mode via the perpendicular electric field component (E⊥y). As a combination of preceding two effects, an attenuated transparency peak (0.72 THz) emerges at a 45° polarization angle. In brief, when the polarization angle $\theta = 0°$, the PIT mode can be excited. With the increase of polarization angle θ, the PIT mode fades gradually and the dipole mode is enhanced. We also want to emphasize that, in this paper, the parameter of AHR is designed carefully to let the frequency of the transparency peak ($\theta = 0°$) coincide with the resonant frequency of the dipole mode ($\theta = 90°$).

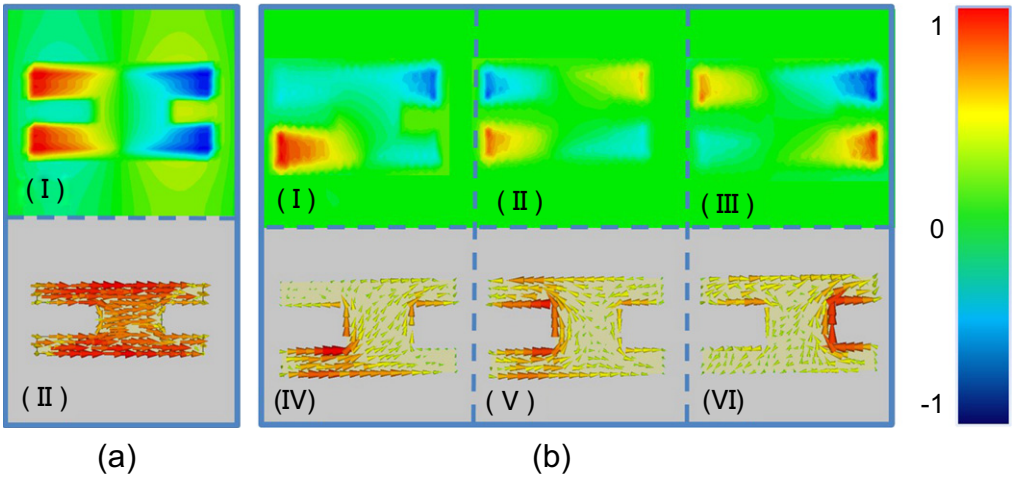

Figure 5. (a) (I) and (II) are the electric field and surface current distributions with a 90° polarization angle. (b) The electric field and surface current distributions with 45° polarization angle. (I) and (IV) at the first resonance dip at 0.66 THz, (II) and (V) at the transparency peak at 0.72 THz, (III) and (VI) at the second resonance dip at 0.78 THz.

Therefore, with the increase of polarization angle θ, the phenomenon that transmission peak (0.72 THz) at $\theta = 0°$ falls down rapidly not only comes from the degeneration of PIT mode, but also contributes to the strong enhanced dipole mode with the transmission dip designed at 0.72 THz. The transmission response at 0.72 THz can be transformed from the transparency peak (switch-on state) to stop band (switch-off state) by varying the polarization angle easily due to the combination effects of reduced PIT mode and enhanced dipole mode. By borrowing this simple polarization control, the AHR meta-atoms structure can be used as a tunable filter.

3.2. Manipulation of dark-mode resonance intensity by different coupling strength

To further understand the effect of coupling in an AHR structure, we change the coupling strength by varying distance d between resonators. Figure 6 presents the transmission spectra with different central bar distance d varying from 10 μm to 40 μm with 10 μm steps. With the increase of bar distance d, resonance frequency blue shifts for bright mode (the low-frequency resonance dip) and red shifts for dark mode (the high-frequency resonance dip). The resonance frequency of dark mode is located at 0.78 THz, 0.79 THz, 0.80 THz, and 0.82 THz with decreased distance d changed from 40 μm to 10 μm with 10 μm steps, respectively. These results agree with the resonance hybridization model in which the resonance energies shift from the initial resonance energies of the resonators with increased coupling. However, the resonance intensity of dark mode damps gradually and the transmission window becomes broad with decreased coupling distances. This observed behavior is different from the proposed two separated back-to-back coupled split-ring resonators (SRRs) for which the reduced coupling distance resulted in closer resonance modes [30].

To clarify the coupling mechanism of different coupling distances, magnetic field and surface current distributions of the high-frequency resonance dip (dark mode) with different

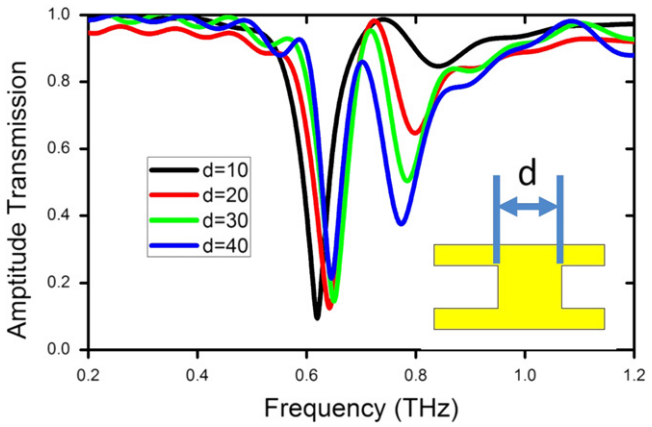

Figure 6. (a) The transmission spectra by varying central bar height d. The insert image is the view of the changed distance d.

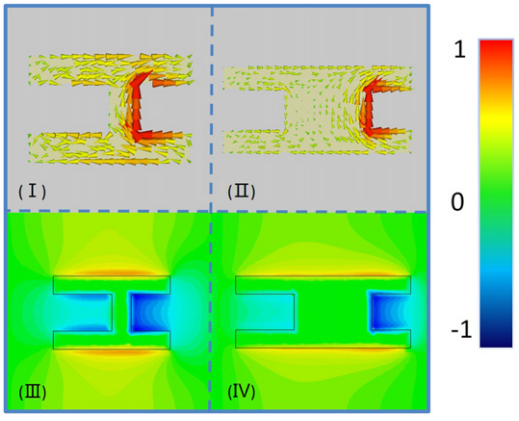

Figure 7. The magnetic field and surface current distributions of the high-frequency resonance dips (I) and (III) at 0.82 THz with d = 10 μm, (II) and (IV) at 0.78 THz with d = 40 μm.

distances, 10 μm and 40 μm, are given in figure 7. The high-frequency resonance is mainly evoked by the right shallower resonator. And more remarkable, the coupled magnetic field intensity concentrates more on the two sides of the arms,

which is different from un-contacted two back-to-back coupled resonators whose intensity concentrated around the resonance cavity [30]. The coupling intensity of closed distance d = 10 μm (see figures 7 (I) and (III)) is stronger than far distance d = 40 μm (see figures 7 (II) and (IV)). Thus, more energies transfer to the deeper side with decreased bar distance, which crippled the intensity of high-frequency resonance. Meanwhile, the transparency window widens with decreased coupling distance. Therefore, the resonance intensity of dark mode can be manipulated from strong to weak simply by controlling the coupling strength with varying distances.

4. Conclusion

In conclusion, we have proposed and demonstrated the tunable PIT effects from two methods based on AHR meta-atom structure. The tunable PIT effect is realized via varying polarization angle and coupling distances. First, the PIT mode and dipole mode are observed to be excited by an incident plane wave with a 0° and 90° polarization angle, respectively. By carefully designing the parameter of the AHR structure to let the resonance frequencies of the PIT mode and dipole mode coincide with each other, the transition from the switch-on state (PIT mode) to switch-off state (dipole mode) is theoretically and experimentally demonstrated by simply adjusting the polarization angle. Then, the manipulation of dark-mode resonance intensity from strong to weak is achieved by various coupling strength with different coupling distances, which provides an insight into the coupling mechanism. Prospectively, due to its special tunable characteristics, the AHR meta-atom structure may be widely used in slow slight, filters, and switch devices.

Acknowledgments

This work was partly supported by the National Program on Key Basic Research Project of China (973 Program, 2014CB339806), the Basic Research Key Project (12JC1407100), the Major National Development Project of Scientific Instrument and Equipment (2011YQ150021 and 2012YQ14000504), the National Natural Science Foundation of China (11174207, 61138001, 61205094 and 61307126), the Shanghai Rising-Star Program (14QA1403100), the Program of Shanghai Subject Chief Scientist (14XD1403000), and the New Century Excellent Talents Project from the Ministry of Education (NCET-12-1052).

References

[1] Zhang S, Park Y, Li J, Lu X, Zhang W and Zhang X 2009 Negative refractive index in chiral metamaterials *Phys. Rev. Lett.* **102** 023901

[2] Paul O, Imhof C, Reinhard B, Zengerle R and Beigang R 2008 Negative index bulk metamaterial at terahertz frequencies *Opt. Express* **16** 6736–44

[3] Tao H, Landy N, Bingham C, Zhang X, Averitt R and Padilla W 2008 A metamaterial absorber for the terahertz regime: design, fabrication and characterization *Opt. Express* **16** 71–81

[4] Tao H, Bingham C, Strikwerda A, Pilon D, Shrekenhamer D, Landy N, Fan K, Zhang X, Padilla W and Averitt R 2008 Highly flexible wide angle of incidence terahertz metamaterial absorber: design, fabrication, and characterization *Phys. Rev.* B **78** 2–5

[5] Paul O, Reinhard B, Krolla B, Beigang R and Rahm M 2010 Gradient index metamaterial based on slot elements *Appl. Phys. Lett.* **96** 241110

[6] Chen L, Zhu Y, Zang X, Cai B, Li Z, Xie L and Zhuang S 2013 Mode splitting transmission effect of surface wave excitation through a metal hole array *Light Sci. Appl.* **2** e60

[7] Chen L, Truong K, Cheng Z, Li Z and Zhu Y , 2014 Characterization of photonic bands in metal photonic crystal slabs *Opt. Commun.* **333** 232–6

[8] Cai W, Chettiar U, Kildishev A and Shalaev V , 2007 Optical cloaking with metamaterials *Nat. Photon.* **1** 224–7

[9] Harris S 2008 Electromagnetically induced transparency *Phys. Today* **50** 36–42

[10] Harris S E, Field J and Imamoğlu A 1990 Nonlinear optical processes using electromagnetically induced transparency *Phys. Rev. Lett.* **64** 1107

[11] Zhang X, Li Q, Cao W, Gu J, Singh R, Tian Z, Han J and Zhang W 2013 Polarization-independent plasmon-Induced transparency in a fourfold symmetric terahertz metamaterial *IEEE J. Sel. Top. Quant.* **19** 8400707

[12] Zhu Z, Yang X, Gu J, Jiang J, Yue W, Tian Z, Tonouchi M, Han J and Zhang W 2013 Broadband plasmon induced transparency in terahertz metamaterials *Nanotechnology* **24** 214003

[13] Zhang F, Zhao Q, Zhou J and Wang S 2013 Polarization and incidence insensitive dielectric electromagnetically induced transparency metamaterial *Opt. Express* **21** 19675–80

[14] Zhang K, Wang C, Qin L, Peng R, Xu D, Xiong X and Wang M 2014 Dual-mode electromagnetically induced transparency and slow light in a terahertz metamaterial *Opt. Lett.* **39** 3539–942

[15] Gu J *et al* 2012 Active control of electromagnetically induced transparency analogue in terahertz metamaterials *Nat. Commun.* **3** 1151

[16] Cao W, Singh R, Zhang C, Han J, Tonouchi M and Zhang W 2013 Plasmon-induced transparency in metamaterials: active near field coupling between bright superconducting and dark metallic mode resonators *Appl. Phys. Lett.* **103** 101106

[17] Singh R, Rockstuhl C, Lederer F and Zhang W L 2009 Coupling between a dark and a bright eigenmode in a terahertz metamaterials *Phys. Rev.* B **79** 085111

[18] Cao W, Singh R, Al-Naib I, He M, Taylor A J and Zhang W 2012 Low-loss ultra-high-Q dark mode plasmonic fano metamaterials *Opt. Lett.* **37** 3366–8

[19] Singh R, Cao W, Al-Naib I, Cong L, Withayachumnankul W and Zhang W 2014 Ultrasensitive terahertz sensing with high-Q fano resonances in metasurfaces *Appl. Phys. Lett.* **105** 171101

[20] Singh R, Al-Naib I, Chowdhury D, Cong L, Rockstuhl C and Zhang W 2014 Probing the transition from an uncoupled to a strong near-field coupled regime between bright and dark mode resonators in metasurfaces *Appl. Phys. Lett.* **105** 081108

[21] Sun S L, He Q, Xiao S Y, Xu Q, Li X and Zhou L 2012 Gradient-index meta-surfaces as a bridge linking propagating waves and surface waves *Nat. Mater.* **11** 426–31

[22] Qu C, Xiao S, Sun S, He Q and Zhou L 2013 A theoretical study on the conversion efficiencies of gradient meta-surfaces *EPL* **101** 54002
[23] Han S, Yang H and Guo L 2013 Ultra-broadband electromagnetically induced transparency using tunable self-asymmetric planar metamaterials *J. Appl. Phys.* **114** 163507
[24] Cheng Z, Chen L, Zang X, Cai B, Peng Y and Zhu Y 2015 Ultrathin dual-mode filtering characteristics of terahertz metamaterials with electrically unconnected and connected U-shaped resonators array *Opt. Commun.* **342** 20–5
[25] Chen L, Gao C, Xu J, Zang X, Cai B and Zhu Y 2013 Observation of electromagnetically induced transparency-like transmission in terahertz asymmetric waveguide-cavities systems *Opt. Lett.* **38** 1379–81
[26] Chen L, Xu J, Gao C, Zang X, Cai B and Zhu Y 2013 Manipulating terahertz electromagnetic induced transparency through parallel plate waveguide cavities *Appl. Phys. Lett.* **103** 251105
[27] Chen L, Cheng Z, Xu J, Zang X, Cai B and Zhu Y 2014 Controllable multiband terahertz notch filter based on a parallel plate waveguide with a single deep groove *Opt. Lett.* **39** 4541–4
[28] Born N, Al-Naib I, Jansen C, Ozaki T, Morandotti R and Koch M 2014 Excitation of multiple trapped-eigenmodes in terahertz metamolecule lattices *Appl. Phys. Lett.* **104** 101107
[29] Chen L, Cao Z, Ou F, Li H, Shen Q and Qiao H 2007 Observation of large positive and negative lateral shifts of a reflected beam from symmetrical metal-cladding waveguides *Opt. Lett.* **32** 1432–4
[30] Aydin K, Pryce I and Atwater H 2010 Symmetry breaking and strong coupling in planar optical metamaterials *Opt. Express* **18** 13407–17